3D Printed Microfluidic Devices for Solid-Phase Extraction and On-Chip Fluorescent Labeling of Preterm Birth Risk Biomarkers

Anna V. Bickham†, Chao Pang†, Benjamin Q. George†, David J. Topham†, Jacob B. Nielsen†, Gregory P. Nordin‡, Adam T. Woolley†*

† Department of Chemistry and Biochemistry, Brigham Young University, Provo, UT, 84602, USA

‡ Department of Electrical and Computer Engineering, Brigham Young University, Provo, UT, 84602, USA

*Corresponding Author: Professor Adam T. Woolley; atw@byu.edu

Abstract

Solid-phase extraction (SPE) is a general preconcentration method for sample preparation that can be performed on a variety of specimens. The miniaturization of SPE within a 3D printed microfluidic device further allows for fast and simple extraction of analytes, while also enabling integration of SPE with other sample preparation and separation methods. Here, we present the development and application of a reversed-phase lauryl methacrylate-based monolith, formed in 3D printed microfluidic devices, which can selectively retain peptides and proteins. The effectiveness of these SPE monoliths and 3D printed microfluidic devices was tested using a panel of nine preterm birth biomarkers of varying hydrophobicities and ranging in mass from 2-470 kDa. The biomarkers were selectively retained, fluorescently labeled, and eluted separately from the excess fluorescent label in 3D printed microfluidic systems. These are the first results demonstrating microfluidic analysis processes on a complete panel of preterm birth biomarkers, an important step toward developing a miniaturized, fully integrated analysis system.

Over the past 30 years, the field of microfluidics has established advantages of low sample and reagent consumption, fast analyses, and cost-effectiveness compared to many benchtop instruments and processes. These benefits are apparent in a variety of applications, including biomarker,[1] nucleic acid,[2] organ-on-a-chip,[3] single- and multi-cellular,[4-5] polymerase chain reaction,[6] and biosensor[7] analyses. Available microfabrication methods have previously limited the design capabilities of these microfluidic devices,[8] but the recent trend towards use of 3D printing has created new possibilities for researchers to miniaturize, iteratively customize, and integrate more sample preparation and analysis methods into fluidic chips.[9] Although the commercial availability of 3D printers capable of producing <100-μm channels is still limited,[10] this barrier can be breached to achieve enclosed, truly microfluidic features.[11]

For growing applications in microfluidics, there is a persistent need to detect lower analyte concentrations. Indeed, the use of small sample volumes in microchannels has a major influence on the approach needed for detection of analytes of interest.[12] Often, lowering the analyte limit of detection must begin during sample preparation by limiting losses and implementing preconcentration. Although there are many methods for preconcentration,[12] solid-phase extraction (SPE) is one of the most general ones, because it can be applied to relatively larger sample volumes.[13] Miniaturization of an SPE system allows for integration with other analysis steps and can be simple, fast, and effective. Many different SPE systems have been developed previously for microfluidic applications, including for analysis of alkaloids,[14] metal ions,[15-16] nucleic acids,[17-19] aromatic hydrocarbons,[20] and phosphopeptides.[21] These applications often utilize a variety of SPE sorbent beds such as packed beads, micro- or nanofibers, porous polymer monoliths, membranes, or other microstructures to achieve high surface areas and appropriate chemical properties for effective extraction.[17,22] Monoliths can be particularly useful

because of their ease of *in situ* fabrication and morphological tuning.[23] Recent initial studies utilized monoliths in 3D printed fluidic devices for hydrogen/deuterium exchange,[24] immunoaffinity extraction,[25] liquid chromatography,[26] and SPE of alkyl esters on a gold nanoparticle modified monolith.[27] However, only for the immunoaffinity extraction were the 3D printed channels truly microfluidic, with cross sections smaller than 100 x 100 μm^2.

Each year, nearly 15 million infants are born prematurely, resulting in over 1 million deaths worldwide from either the direct effects of preterm birth (PTB) or later complications, such as respiratory difficulties or increased susceptibility to infection.[28] The World Health Organization has a number of recommended interventions to reduce mortality rates,[28] but they are mainly focused on care during labor and after delivery. In part, this is because no early clinical assessment currently exists to give warning of an imminent PTB prior to the onset of labor. Such an assessment may be possible with a panel of nine previously discovered protein and peptide biomarkers,[29] summarized in Table 1. Toward development of a PTB risk assessment, some of these protein and peptide biomarkers have been evaluated in microfluidic devices for immunoaffinity extraction,[25,30] electrophoretic separations,[31-32] and SPE.[33-34] However, this entire panel has not previously been evaluated in a microfluidic analysis format.

Here, we show the development of a reversed-phase monolith for SPE of PTB biomarkers. These monoliths are photopolymerized within 3D printed microfluidic device channels, allowing for easy and fast device fabrication. The SPE devices were evaluated for retention and elution of nine PTB biomarkers as well as a fluorescent label, Alexa Fluor 532 NHS ester. Finally, these 3D printed microfluidic devices were tested, using the same nine PTB biomarker analytes, for performing on-chip SPE and fluorescent labeling. Notably, these 3D printed devices and reversed-phase monoliths are well-suited for SPE retention and elution of

PTB biomarkers during on-chip labeling. Our results demonstrate nearly universal retention and elution performance for SPE of a diverse panel of protein and peptide biomarkers, marking an important step toward the development of a complete miniaturized PTB risk assessment.

MATERIALS AND METHODS

Materials. The following chemicals were ordered from Sigma (St. Louis, MO): poly(ethylene glycol) diacrylate (PEGDA; MW 250 Da), phenylbis(2,4,6-trimethylenzoyl)phosphine oxide (Irgacure 819), acetonitrile (ACN), 1-dodecanol, ethylene dimethacrylate (EDMA), lauryl methacrylate (LMA), octyl methacrylate (OMA), 2,2-dimethoxy-2-phenylacetophenone (DMPA), 3-(trimethoxysilyl)propyl methacrylate, and dimethyl sulfoxide (DMSO). PTB biomarkers were purchased from the following sources: PTB peptides 1-3 (synthesized by Biomatik, Wilmington, DE; see Table S1), corticotropin-releasing factor (CRF, GenScript, Piscataway, NJ), defensins (mixed human neutrophil peptides, Athens Research and Technology, Athens, GA), ferritin (EMD Millipore, Billerica, MA), lactoferrin (Sigma), tumor necrosis factor-α receptor type 1 (TNF, ProSpec, East Brunswick, NJ), thrombin and antithrombin (Haematologic Technology, Essex Junction, VT), and heparin (Alfa-Aesar, Haverhill, MA). Fluorescent labeling of biomarkers was performed using Alexa Fluor 532 NHS ester (Thermo Fisher, Fair Lawn, NJ) with filtering in Amicon Ultra 0.5 mL centrifugal cutoff filters (EMD Millipore). Bicarbonate buffer (BCB, pH 10) was prepared using sodium bicarbonate from Merck (Darmstadt, Germany) and sodium hydroxide from Mallinckrodt Baker (Paris, KY). 2-nitrophenyl phenyl sulfide (NPS, TCI Chemicals, Portland, OR) and glass slides (25 mm x 75 mm x 1 mm; VWR, Center Valley, PA) were purchased for 3D printing. Additional

solvents of isopropyl alcohol (IPA) and toluene came from Macron. Finally, all water was purified to 18.3 MΩ·cm prior to use (Barnstead EASY-Pure UV/UF, Dubuque, IA).

3D Printing. Microfluidic devices are designed in the freeware computer-aided design (CAD) software, OpenSCAD (openscad.org); each print has 10-µm-thick layers and includes five identical devices. The design is adapted from one used by Parker et al.[25] A 6-pixel (46 µm) by 5-layer (50 µm) channel connects a 2.7 mm diameter x 0.75 mm deep reservoir to a 1.1 mm diameter horizontal port, into which PTFE tubing (0.022 in ID x 0.042 in OD; Cole Parmer, Vernon Hills, IL) is inserted for the application of vacuum for flow through the channel. The device also includes a 600 µm wide monolith polymerization window, placed 60 µm above the channel.[25] CAD designs of the devices can be seen in Figure 1A-B.

Microfluidic devices were formed in a custom 3D printer with a 385 nm light source. The development of this printer and corresponding custom resin, consisting of 2% NPS and 1% Irgacure 819 in PEGDA, have been described previously.[11] The exposure time for each layer in the bulk material was 600 ms with 200 ms less exposure in the 3 pixels (~22 µm) to the side of and 3 layers (~30 µm) above the channel region to widen the channels (70 µm x 50 µm) beyond the designed size, as detailed previously by Beauchamp et al.[35] All 3D prints were exposed with a measured optical irradiance of 21 $mW \cdot cm^{-2}$ in the image plane.

Monolith Preparation. Similar to previously described procedures,[33-34,36] reversed-phase monolithic columns were prepared using 1% DMPA photoinitiator in a mixture of monomer (LMA or OMA), crosslinker (EDMA), and porogens (1-dodecanol and/or cyclohexanol). Initially, these mixtures were polymerized in microcentrifuge tubes for 10 min under a UV lamp (Uvitron, West Springfield, MA) to analyze the degree of photopolymerization in each mixture. Analysis was performed by visual inspection. Once a suitable range of component compositions

was identified using this approach, mixtures were polymerized in 3D printed device channels. No channel surface treatment prior to monolith formation was required. After photopolymerization, some channels were sectioned with a razor blade and imaged using SEM[25] (Helios Nanolab 600 FEI, Fisher), and others were experimentally tested by performing SPE of a PTB biomarker. SEM images were analyzed using Image J software (NIH; imagej.nih.gov) to determine average pore and nodule sizes. Each monolith formulation was analyzed for flow when vacuum was applied; morphology of nodules and pores; and PTB biomarker extraction, retention, and elution. These criteria allowed for a well-suited mixture to be decided upon and used for SPE and on-chip labeling of all nine PTB biomarkers. Experimental procedures for contact angle measurements of OMA:EDMA and LMA:EDMA mixtures are given in the Supporting Information.

After polymerization of monoliths within the 3D printed device channels, PTFE tubing was inserted into the horizontal port for each channel and affixed with hot glue, then IPA was drawn by vacuum through each channel for a minimum of 30 min. Cleaning was complete when a channel and monolith could be successfully brought to complete dryness by vacuum. If residual liquid could not be removed by vacuum, additional IPA, device heating to ~35 °C, and vacuum were applied. Monoliths in microfluidic devices prepared in this manner could then be stored under ambient conditions until use.

Experimental Setup. PTB biomarkers were fluorescently labeled and filtered using previously described procedures[32,37] for prelabeled biomarker experiments. Thrombin-antithrombin complex (TAT) was prepared 24 h prior to fluorescent labeling.[32] For on-chip labeling experiments, PTB biomarkers were diluted to the desired concentration in 10 mM BCB.

SPE experiments were performed in a previously described microscope setup for laser-induced fluorescence detection.[25,37] Fluorescence images were collected with either a Photometrics Cool-SNAP HQ2 CCD camera (Tucson, AZ) or a Hamamatsu ORCA-Fusion CMOS camera (Bridgewater, NJ). Prior to biomarker extraction, a monolith was prepared by adding IPA to the reservoir and allowing the channel to fill to the monolith by capillary action. Next, the IPA was replaced with 10 mM BCB (pH 10) and vacuum was applied for 3 min. Then, the liquid in the reservoir was replaced with 30% ACN (in 10 mM BCB), with vacuum application for 90 s. Finally, the same was done with 90% ACN for another 90 s. This process of flowing buffer, 30% ACN, and 90% ACN was repeated three times to clean and equilibrate the channel. The flow rate was estimated to be 0.5-1 μL/min by monitoring the emptying time for a measured volume of fluid in filled reservoirs.

After equilibration, SPE experiments were performed. For prelabeled biomarkers, vacuum was used to drive the following flow steps: BCB for 3 min, sample loading for 90 s, BCB buffer rinse three times for 90 s each, 30% ACN for 90 s, and 90% ACN for 90 s. Although most analytes were tested at several concentrations, the following concentrations were used for each analyte for the reported data: ferritin, 10 nM; TNF, 100 nM; peptide 1, 500 nM; defensins, 200 nM; CRF, peptides 2-3, TAT, and lactoferrin 1 μM; and Alexa Fluor, 2 μM. For on-chip labeling experiments, a similar procedure was performed except two loading steps were performed (PTB biomarker for 90 s, then Alexa Fluor labeling solution for 90 s) followed by a 30 min incubation prior to the buffer rinse. During the incubation time, the reservoir was refilled with labeling solution as needed to prevent evaporative drying. For the reported data, the following concentrations were used for each analyte: peptide 1, 500 nM; CRF, 1 μM; peptides 2-3, 600 nM; defensins, 200 nM; lactoferrin, 60 nM; TNF, 100 nM; TAT and ferritin, 50 nM; and

Alexa Fluor, 20 μM. For this fundamental study, biomarker concentrations are higher than reported clinically relevant levels[29] to allow easy signal detection during retention and elution. The analyte enrichment capabilities of our approach should allow future studies with biomarker concentrations at or below the reported action levels.

After each flow step, a fluorescence image was captured using 200 ms exposure (for both detectors). All images were analyzed using Image J to obtain the fluorescent signal present on the monolith after each step of the process. The background signal was subtracted from each, then the values were normalized to the signal after sample loading for each experiment. Average signals from three replicates for each experiment are reported.

Many protein hydrophobicity calculation algorithms exist that account for both amino acid sequence and protein tertiary structure.[38] For this study, calculations for biomarker hydrophobicity were performed using the amino acid sequence of each biomarker and an online hydrophobicity index (www.peptide2.com/N_peptide_hydrophobicity_hydrophilicity.php). Because retained analytes were dissolved in pH 10 solutions where some denaturation may occur, hydrophobicity differences due to tertiary structure were not considered.

RESULTS AND DISCUSSION

3D printed microfluidic devices for SPE were based on a design used previously by Parker et al.[25] However, the design was changed slightly by creating a horizontal port for attachment of external tubing, which allowed for easier interfacing with vacuum to drive fluid flow (Figure 1A-C). Because 3D printing was used for device fabrication, design modifications were straightforward to apply; the CAD design could be edited, and new devices could be 3D printed in less than 30 min. As reported previously, these devices absorb UV light strongly (h_a =

10.8 μm at 385 nm)[11] but have high transmittance for visible wavelengths (99.8% transmittance at 532 nm).[31]

Although several similar reversed-phase monolith formulations have been reported previously,[33-34,36] a new formulation was developed for these SPE experiments both to improve formation consistency and to avoid the use of Tween-20, which can be incorporated into the monolith during polymerization and unnecessarily complicates monolith formulation as an additional component. For initial development of the new monolith, a number of mixtures containing OMA (10-28%), EDMA (7-25%), 1-dodecanol (45-70%), cyclohexanol (0-12%), and DMPA (1%) were mixed and polymerized in microcentrifuge tubes. Our initial choice of OMA was based on previous work where it provided suitable monolith hydrophobicity to selectively retain and elute protein biomarkers.[36,39] Visual inspection found that mixtures containing too high of a porogen content (not enough monomer and crosslinker) were viscous and transparent, while mixtures that did not contain enough porogens (too much monomer and crosslinker) were also transparent from lack of a porous structure. The most opaque mixtures were judged to have formed the most porous monolithic structures; these occurred when the total porogen content was 60-70% and the EDMA crosslinker accounted for at least 15% of the mixture.

Using these results, another series of mixtures containing the same components was prepared (Table 2), placed in 3D printed microfluidic channels for polymerization and imaged with SEM (Figure 2). From the formation and flow properties of these monoliths, several observations can be made. First, monoliths that contained a higher porogen (1-dodecanol and cyclohexanol) content had higher flow rates than those with lower porogen content: the flow rates of monolith formulations A-B were slower than those of formulations C-D, which were slower than those of formulations E-F. This meant that after polymerization was complete, it was

more difficult to clear the unpolymerized material from monolith formulations A-B than formulations E-F. Thus, those low-porogen-content monoliths (formulations A-B) were judged too dense for use in SPE experiments.

A second observation from the Figure 2 images is distinct morphological differences when the entire porogen content is comprised of 1-dodecanol (Figure 2, right column) instead of if the mixture also contains 10% cyclohexanol (Figure 2, left column). We expected that the use of only 1-dodecanol would result in a greater number of smaller pores whereas the addition of cyclohexanol would result in fewer, but larger pores due to greater solubility of the OMA monomer in dodecanol.[40] However, these images suggest that the effects of these porogens may be more complex; morphological differences from porogen content, while significant, did not follow a simple trend.

A further observation from monolith formulations G-L is the effect of maintaining constant porogen content while changing the ratio of OMA to EDMA (monomer to crosslinker). Figure 2G-H shows, similar to the microcentrifuge tube experiments described earlier, that monolith formation is inconsistent when there is not enough crosslinker present in the mixture. Thus, we see in these images that the monoliths are dense in some regions while other areas lack a monolith structure. We also observe that as the crosslinker concentration increases, the monolith pore and nodule sizes also increase (compare the Table 2 pore and nodule sizes for monolith formulations I-J with K-L). This is likely because the greater number of reactive groups in EDMA draws the polymerizable units in the mixture into a larger, more rigid structure than when a higher percentage of OMA is present. These results indicate that the nodule and pore sizes, and thus the total surface area of the monolith, are tunable by changing the ratio of polymerizable groups in the monomer and crosslinker components.

The results in Figure 2 and Table 2 confirmed that several mixtures were good candidates for performing SPE. Specifically, monolith formulations C, F, J, and L appeared to be most promising, with good morphology and high surface area. To simplify the mixture, formulation C was excluded as it required two porogens. The remaining three monoliths were tested using a simple SPE experiment. We found that the vacuum-driven flow rate through monoliths from formulation F was too high for efficient extraction to occur due to insufficient interaction between the monolith surface and PTB-related analytes. Although a smaller pressure drop might be able to slow the flow rate enough to correct this, no additional experiments were performed with this mixture or to quantitatively determine an optimal flow rate for extraction. Extraction was also inefficient for monoliths from formulation L, likely due to the low percentage of OMA in this formulation; the monolith was not hydrophobic enough to effectively extract ferritin, a model PTB protein biomarker.

The 15% OMA, 20% EDMA, and 65% 1-dodecanol monolith formulation was used in initial SPE experiments. Although the flow rate and hydrophobicity of this monolith were sufficient for extraction of ferritin, it did not allow for selective elution of excess fluorescent dye prior to the biomarker. For example, flow of just 30% ACN led to partial elution of ferritin. These results indicated that a more hydrophobic monolith was needed to retain all PTB biomarkers, particularly the smaller peptides. Since increasing the OMA percentage detrimentally altered the monolith morphology, instead, the OMA in the monolith from Figure 2J was replaced with LMA. This change had no noticeable effect on monolith morphology (compare Figure 1E with Figure 2J) but increased the hydrophobicity of the monolith (see contact angle data in Table S2) enough to allow for PTB biomarker SPE with selective retention and elution. This LMA monolith was also found to have consistent attachment to the 3D printed

channel surfaces (Figure 1D) and was well-confined to the polymerization window (Figure 3A). With these encouraging results, no additional monolith optimization was performed with LMA-containing formulations.

With a suitable monolith formulation, the 3D printed microfluidic devices were ready for SPE experiments. In initial studies, we found that a fluorescent byproduct of Irgacure 819, the photoinitiator used during 3D printing, was present in the devices and soluble in the ACN eluent. This fluorescent impurity increased the background signal during point fluorescence detection experiments; however, imaging of fluorescence on the monoliths allowed effective monitoring of analyte present during extraction and elution without interference from the impurity.

Using fluorescent imaging detection, the signal after the loading and elution of analytes could be monitored. We selected ferritin as a model biomarker analyte because its large size was expected to lead to strong retention on the reversed-phase monolith. To evaluate conditions for on-chip labeling, Alexa Fluor dye was used as another analyte for initial comparisons. The BCB (pH 10) used for loading also corresponds to the elution buffer of an immunoaffinity extraction system described earlier.[25] This matching of immunoaffinity eluent to SPE loading solution should facilitate integration of these two processes in a future PTB risk diagnostic.

The rinsing and elution solvents for Alexa Fluor and Alexa Fluor-labeled ferritin were chosen to allow for selective elution of the two analytes. Selective elution is essential for on-chip labeling and should also allow biomarkers to be eluted in a small-volume, concentrated plug. Such an enriched band should help to lower limits of detection and enable heart-cut injection for subsequent microchip electrophoresis.[31,33] Similar to previous studies,[33-34] we found that Alexa Fluor could be eluted with only buffer or at low ACN concentrations. In contrast, the ferritin was strongly retained until 90% ACN was flowed through the monolith, at which time significant

elution could be observed. Figure 3B shows representative images for both Alexa Fluor and ferritin elution. In each case, almost no fluorescent signal can be seen on the monolith during the buffer equilibration prior to sample loading. After loading, both monoliths show high fluorescent signal. In the Alexa Fluor experiments, the fluorescent signal is removed with buffer and 30% ACN, such that almost no fluorescent signal is visible in the image after 30% ACN flow. This indicates limited retention of Alexa Fluor with almost no material remaining after flowing 30% ACN. In contrast, the ferritin images show that the high fluorescent signal is maintained through the buffer and 30% ACN steps, demonstrating that ferritin is well retained. Lastly, the fluorescent signal on the monolith is lower after the 90% ACN elution, indicating good elution of the analyte and selective retention of ferritin compared to Alexa Fluor dye.

To show the versatility of this SPE system for additional analytes, a panel of nine PTB risk biomarkers (Table 1) was evaluated. These peptides and proteins were fluorescently labeled off chip, loaded on reversed-phase LMA monoliths using the established conditions, and then observed by fluorescence imaging after retention and elution. Figure 4A shows the relative fluorescent signal present on the monoliths for each analyte after loading and flowing buffer and two different percentages of ACN, demonstrating the retention and elution characteristics of the PTB biomarkers and fluorescent label. Figure 4B shows the percentage of each retained analyte eluted with 90% ACN. Of the nine proteins and peptides, four were well retained during the buffer rinse and 30% ACN flow through steps, with >60% of the total captured material eluted during the 90% ACN step. Three additional biomarkers were moderately retained, with >30% of the total captured material eluted with 90% ACN. The final three analytes, Alexa Fluor, peptide 1, and defensins, were largely eluted during the buffer rinse step, indicating that these analytes were not strongly retained on the monolith.

As the conditions for the elution of analytes from these monoliths were chosen to selectively elute Alexa Fluor dye and retain ferritin, it is not surprising that different retention properties were seen for other analytes. We expected retention to correlate with the size of the analyte, with large proteins well retained and small peptides having less retention. Table 1 shows that the panel of PTB biomarkers has more than a 100-fold range in masses and considerable variation in hydrophobic nature. Thus, the limited retention of peptide 1 was likely because of its small size, and the low retention of defensins was likely due to the higher relative hydrophilicity within its amino acid sequence. However, the remaining seven biomarkers were moderately or well retained, showing that this SPE system has potential to perform selective extraction through retention and elution of many proteins and peptides.

With these encouraging results for SPE of prelabeled proteins and peptides, we focused on coupling SPE with an on-chip fluorescent labeling reaction. In contrast with the previous experiments where PTB biomarkers were fluorescently labeled overnight in microcentrifuge tubes prior to extraction experiments, unlabeled biomarkers were loaded onto the monolith followed by labeling with Alexa Fluor at room temperature for 30 min prior to performing the rinsing and elution steps. Similar to Figure 4, Figure 5A shows relative fluorescence signal from monoliths after each step in the process for all 9 biomarkers plus the fluorescent label, whereas Figure 5B further shows the percentage of each retained analyte that was eluted with 90% ACN. Analysis of these elution percentages shows moderate to good selectivity for 90% ACN elution of all nine biomarkers relative to the Alexa Fluor label, whose elution is complete in 30% ACN. These results show the ability to perform on-chip fluorescent labeling of proteins and peptides having a variety of masses and hydrophobicities, with selective retention relative to the fluorescent dye. Importantly, our results also demonstrate the first use of 3D printed devices for

on-chip labeling and purification of an entire panel of PTB biomarkers. Our data further establish the ability to achieve good retention of all nine PTB biomarkers in SPE combined with selective elution of excess dye prior to biomarker elution, all under identical conditions, a key step for streamlined on-chip sample preparation.

Our work with on-chip labeling in Figure 5 also shows that, unlike for the prelabeled biomarkers (Figure 4), retention for peptide 1 and defensins is significantly increased compared to the fluorescent dye. Additionally, some biomarkers including TNF and defensins showed incomplete elution with 90% ACN, as demonstrated by residual fluorescent signal (Figure 5A). We hypothesized that these differences were due to the longer (30 min) labeling/incubation time, which increased interaction with the reversed-phase monolith for retention. To test the effect of the incubation time, peptide 1 prelabeled with Alexa Fluor was loaded with a 30-min extraction period prior to rinsing and elution. This extension of the extraction period raised the percentage of peptide 1 eluted with 90% ACN to >25%, the same as observed for peptide 1 during on-chip labeling experiments. Thus, retention of small or hydrophilic analytes can be improved by increasing extraction time, further extending the utility of our SPE system to a variety of peptide and protein analytes. Although this increased interaction time may result in incomplete elution, it does not prevent future downstream analysis of these PTB biomarkers. Use of a mixed mode sorbent monolith could be investigated in a future study if needed to improve retention of small or hydrophilic analytes without deteriorating elution.

CONCLUSIONS

In this work, we have demonstrated the feasibility of using 3D printed microfluidic devices to combine SPE and fluorescent labeling of nine individual analytes in a disease risk

biomarker panel. The use of 3D printing for fabrication can make such devices widely available to other researchers. Moreover, 3D printing streamlines the integration of microfluidic assay components such as valves and pumps[41] and makes possible the combination of SPE and labeling with further on-chip sample preparation or separation steps, including chromatography or electrophoresis.[25,31,33,34] Future integration of 3D printed, integrated pumps and valves along with point detection should also allow for more thorough tracking of analytes via mass balance calculations. Furthermore, this work is the first to evaluate the entire panel of nine PTB biomarkers in a miniaturized assay, which constitutes an important step toward the development of a complete PTB risk diagnostic. Finally, the ability for these processes to be applied to analytes that have different masses or hydrophobicities demonstrates the broad versatility 3D printed microfluidic SPE systems for use in other peptide- and protein-based analysis applications.

Acknowledgements

We thank NIH for funding of this work (R01 EB027096, and R15 GM123405-01A1). Funding for D.J.T. was provided by the National Science Foundation Chemistry and Biochemistry REU Site to Prepare Students for Graduate School and an Industrial Career under award CHE-1757627.

Notes

The authors declare the following competing financial interest(s): A.V.B., G.P.N. and A.T.W. own shares in Acrea 3D, a company that is commercializing microfluidic 3D printing.

References

1. Sonker, M.; Sahore, V.; Woolley, A. T. Recent advances in microfluidic sample preparation and separation techniques for molecular biomarker analysis: a critical review. *Anal. Chim. Acta* **2017,** *986,* 1-11.
2. Zhang, L.; Ding, B.; Chen, Q.; Feng, Q.; Lin, L.; Sun, J. Point-of-care-testing of nucleic acids by microfluidics. *Trends Anal. Chem.* **2017,** *94,* 106-116.
3. Kimura, H.; Sakai, Y.; Fujii, T. Organ/body-on-a-chip based on microfluidic technology for drug discovery. *Drug Metabol. Pharmacokin.* **2018,** *33,* 43-48.
4. Rothbauer, M.; Zirath, H.; Ertl, P. Recent advances in microfluidic technologies for cell-to-cell interaction studies. *Lab Chip* **2018,** *18,* 249-270.
5. Prakadan, S. M.; Shalek, A. K.; Weitz, D. A. Scaling by shrinking: empowering single-cell 'omics' with microfluidic devices. *Nat. Rev. Genet.* **2017,** *18,* 345-361.
6. Ahrberg, C. D.; Manz, A.; Chung, B. G. Polymerase chain reaction in microfluidic devices. *Lab Chip* **2016,** *16,* 3866-3884.
7. Kim, J.; Campbell, A. S.; de Ávila, B.E.; Wang, J. Wearable biosensors for healthcare monitoring. *Nat. Biotechnol.* **2019,** *37,* 389-406.
8. Wu, J.; Gu, M. Microfluidic sensing: state of the art fabrication and detection techniques. *J. Biomed. Optics* **2011,** *16,* 080901.
9. Nielsen, A. V.; Beauchamp, M. J.; Nordin, G. P.; Woolley, A. T. 3D printed microfluidics. *Annu. Rev. Anal. Chem.* **2020,** *13,* DOI: 10.1146/annurev-anchem-091619-102649.
10. Beauchamp, M. J.; Nordin, G. P.; Woolley, A. T. Moving from millifluidic sub-100-µm cross-section 3D printed devices. *Anal. Bioanal. Chem.* **2017,** *409,* 4311-4319.
11. Gong, H.; Bickham, B. P.; Woolley, A. T.; Nordin, G. P. Custom 3D printer and resin for 18 µm x 20 µm microfluidic flow channels. *Lab Chip.* **2017,** *17,* 2899-2909.
12. Zhao, C.; Ge, Z.; Yang, C. Microfluidic techniques for analytes concentration. *Micromachines* **2017,** *8,* 28.
13. Yu, C.; Davey, M. H.; Svec, F.; Fréchet, J. M. J. Monolithic porous polymer for on-chip solid-phase extraction and preconcentration prepared by photoinitiated in situ polymerization within a microfluidic device. *Anal. Chem.* **2001,** *73,* 5088-5096.
14. Farahani, A.; Sereshti, H. An integrated microfluidic device for solid-phase extraction and spectrophotometric detection of opium alkaloids in urine samples. *Anal. Bioanal. Chem.* **2020,** *412,* 129-138.
15. Park, M.; Seo, T. S. An integrated microfluidic device with solid-phase extraction and graphene oxide quantum dot array for highly sensitive and multiplex detection of trace metal ions. *Biosens. Bioelectron.* **2019,** *126,* 405-411.
16. Wu, Q.; He, J.; Meng, H.; Wang, Y.; Zhang, Y.; Li, H.; Feng, L. A paper-based microfluidic analytical device combined with home-made SPE column for the colorimetric determination of copper(II) ion. *Talanta.* **2019,** *204,* 518-524.

17. Campos, C. D. M.; Gamage, S. S. T.; Jackson, J. M.; Witek, M. A.; Park, D. S.; Murphy, M. C.; Godwin, A. K.; Soper, S. A. Microfluidic-based solid phase extraction of cell free DNA. *Lab Chip* **2018,** *18,* 3459-3470.
18. Mauk, M. G.; Song, J.; Liu, C.; Bau, H. H. Simple approaches to minimally-instrumented, microfluidic-based point-of-care nucleic acid amplification tests. *Biosensors.* **2018,** *8,* 17.
19. Brassard, D.; Geissler, M.; Descarreaux, M.; Tremblay, D.; Dauod, J.; Clime, L.; Mounier, M.; Charlebois, D.; Veres, T. Extraction of nucleic acids from blood: unveiling the potential of active pneumatic pumping in centrifugal microfluidics for integration and automation of sample preparation processes. *Lab Chip* **2019,** *19,* 1941-1952.
20. Zhang, Y.; Xiang, J.; Wang, Y.; Qiao, Z.; Wang, W. A 3D printed centrifugal microfluidic platform for spilled oil enrichment and detection based on solid phase extraction (SPE). *Sens. Actu. B: Chem.* **2019,** *296,* 126603.
21. Deng, J.; Ikenishi, F.; Smith, N.; Lazar, I. M. Streamlined microfluidic analysis of phosphopeptides using stable isotope-labeled synthetic peptides and MRM-MS detection. *Electrophoresis* **2019,** *39,* 3171-3184.
22. Buszewski, B.; Szultka, M. Past, present, and future of solid phase extraction: a review. *Crit. Rev. Anal. Chem.* **2012,** *42,* 198-213.
23. Knob, R.; Sahore, V.; Sonker, M.; Woolley, A. T. Advances in monoliths and related porous materials for microfluidics. *Biomicrofluidics* **2016,** *10,* 032901.
24. Svejdal, R. R.; Dickinson, E. R.; Sticker, D.; Kutter, J. P.; Rand, K. D. Thiol-ene microfluidic chip for performing hydrogen/deuterium exchange of proteins at subsecond time scales. *Anal. Chem.* **2019,** *91,* 1309-1317.
25. Parker, E. K.; Nielsen, A. V.; Beauchamp, M. J.; Almughamsi, H. M.; Nielsen, J. B.; Sonker, M.; Gong, H.; Nordin, G. P.; Woolley, A. T. 3D printed microfluidic devices with immunoaffinity monoliths for extraction of preterm birth biomarkers. *Anal. Bioanal. Chem.* **2019,** *411,* 5405-5413.
26. Gupta, V.; Beirne, S.; Nesterenko, P. N.; Paull, B. Investigating the effect of column geometry on separation efficiency using 3D printed liquid chromatographic columns containing polymer monolithic phases. *Anal. Chem.* **2018,** *90,* 1186-1194.
27. Carrasco-Correa, E. J.; Cocovi-Solberg, D. J.; Herrero-Martínez, J. M.; Simó-Alfonso, E. F.; Miró M. 3D printed fluidic platform in *in-situ* covalently immobilized polymer monolithic column for automatic solid-phase extraction. *Anal. Chim. Acta* **2020,** *1111,* 40-48.
28. *Survive and thrive: transforming care for every small and sick newborn*; World Health Organization: Geneva, 2019.
29. Esplin, M. S.; Merrell, K.; Goldenberg, R.; Lai, Y.; Iams, J. D.; Mercer, B.; Spong, C. Y.; Miodovnik, M.; Simhan, H. N.; van Dorsten, P.; Dombrowski, M. Proteomic identification of serum peptides predicting subsequent spontaneous preterm birth. *Am. J. Obstet. Gynecol.* **2011.** *204,* e1-8.

30. Sonker, M.; Parker, E. K.; Nielsen, A. V.; Sahore, V.; Woolley, A. T. Electrokinetically operated microfluidic devices for integrated immunoaffinity monolith extraction and electrophoretic separation of preterm birth biomarkers. *Analyst.* **2018,** *143,* 224-231.
31. Beauchamp, M. J.; Nielsen, A. V.; Gong, H.; Nordin, G. P.; Woolley, A. T. 3D printed microfluidic devices for microchip electrophoresis of preterm birth biomarkers. *Anal. Chem.* **2019,** *91,* 7418-7425.
32. Nielsen, J. B.; Nielsen, J. B.; Carson, R. H.; Lin, H.-J. L.; Hanson, R. L.; Sonker, M.; Mortensen, D. N.; Price, J. C.; Woolley, A. T. Analysis of thrombin-antithrombin complex formulation using microchip electrophoresis and mass spectrometry. *Electrophoresis* **2019,** *40,* 2853-2859.
33. Sahore, V.; Sonker, M.; Nielsen, A. V.; Knob, R.; Kumar, S.; Woolley, A. T. Automated microfluidic devices integrating solid-phase extraction, fluorescent labeling, and microchip electrophoresis for preterm birth biomarker analysis. *Anal. Bioanal. Chem.* **2018,** *410,* 933-941.
34. Kumar, S.; Sahore, V.; Rogers, C. I.; Woolley, A. T. Development of an integrated microfluidic solid-phase extraction and electrophoresis device. *Analyst.* **2016,** *141,* 1660-1668.
35. Beauchamp, M. J.; Gong, H.; Woolley, A. T.; Nordin, G. P. 3D printed microfluidic features using dose control in X, Y, and Z dimensions. *Micromachines* **2018,** *9,* 326.
36. Yang, R.; Pegaduan, J. V.; Yu, M.; Woolley, A. T. On chip preconcentration and fluorescence labeling of model proteins by use of monolithic columns: device fabrication, optimization, and automation. *Anal. Bioanal. Chem.* **2015,** *407,* 737-747.
37. Nielsen, A. V.; Nielsen, J. B.; Sonker, M.; Knob, R.; Sahore, V.; Woolley, A. T. Microchip electrophoresis separation of a panel of preterm birth biomarkers. *Electrophoresis* **2018,** *39,* 2300−2307.
38. Simm, S.; Einloft, J.; Mirus, O.; Schleiff, E. 50 years of amino acid hydrophobicity scales: revisiting the capacity for peptide classification. *Biol. Res.* **2016,** *49,* 31.
39. Nge, P. N.; Pagaduan, J. V.; Yu, M.; Woolley, A. T. Microfluidic chips with reversed-phase monoliths for solid phase extraction and on-chip labeling. *J. Chromatogr. A* **2012,** *1261,* 129-135.
40. Vlakh, E. G.; Tennikova, T. B. Preparation of methacrylate monoliths. *J. Sep. Sci.* **2007,** *30,* 2801-2813.
41. Gong, H.; Woolley, A. T.; Nordin, G. P. High density 3D printed microfluidic valves, pump, and multiplexers. *Lab Chip* **2016,** *16,* 2450-2458.

Tables

Table 1. PTB biomarkers, their molecular masses, and weighted calculations of the hydrophobicity of their amino acid composition.

Biomarker	Mass (kDa)	Amino Acid Characterization		
		Hydrophobic	Neutral	Hydrophilic
Peptide 1	2.0	58%	21%	21%
CRF	2.7	49%	20%	32%
Peptide 2	4.2	50%	30%	20%
Peptide 3	4.2	48%	30%	23%
Defensins	3-20	41±7%	24±5%	35±6%
TNF	26	38%	38%	24%
Lactoferrin	80	39%	35%	25%
TAT	120	39%	33%	28%
Ferritin	420	37%	33%	30%

Table 2. Formulations, and mean ± standard deviation (each n = 50) nodule and pore sizes for monoliths consisting of 1% DMPA initiator in a mixture of OMA, EDMA, 1-dodecanol, and cyclohexanol. Formulations also correspond to panel letters in Figure 2. Formulations A-F maintained a 1:1 OMA:EDMA ratio while varying the OMA+EDMA:porogen ratio. Formulations G-L maintained a 65% total porogen content while varying the OMA:EDMA ratio.

Monolith Formulation	OMA (%)	EDMA (%)	1-Dodecanol (%)	Cyclohexanol (%)	Average Nodule Size (μm)	Average Pore Size (μm)
A	20	20	50	10	0.14 ± 0.04	0.21 ± 0.09
B	20	20	60		0.89 ± 0.19	0.98 ± 0.58
C	17.5	17.5	55	10	0.91 ± 0.56	1.21 ± 0.34
D	17.5	17.5	65		1.51 ± 0.39	2.19 ± 1.36
E	15	15	60	10	1.48 ± 0.35	2.55 ± 1.04
F	15	15	70		0.41 ± 0.08	0.58 ± 0.24
G	20	15	55	10	n/a	n/a
H	20	15	65		0.32 ± 0.05	0.33 ± 0.17
I	15	20	55	10	0.45 ± 0.07	0.67 ± 0.21
J	15	20	65		0.85 ± 0.13	1.51 ± 0.73
K	10	25	55	10	1.25 ± 0.18	1.87 ± 0.80
L	10	25	65		0.93 ± 0.25	1.50 ± 0.88

Figures

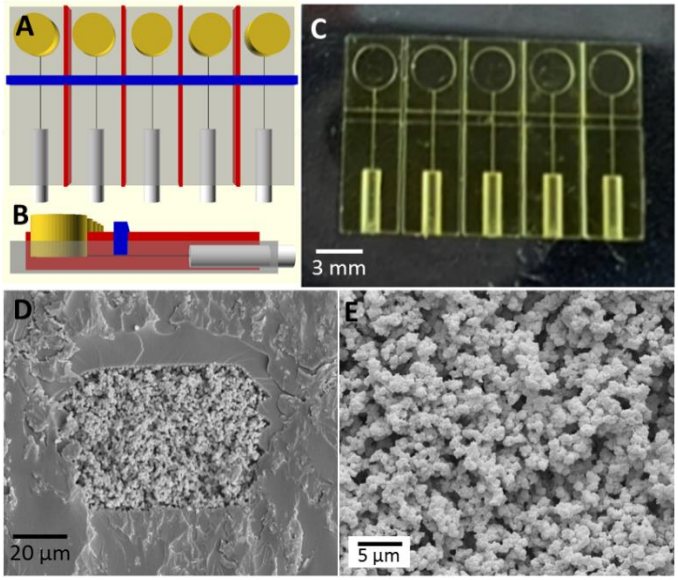

Figure 1. 3D printed microfluidic devices with monoliths for SPE and on-chip labeling experiments. (A-B) Top- and side-views of the CAD design of 3D printed devices, which have five identical channels (light blue) with reservoirs (yellow) and vacuum-attachment ports (gray). A polymerization window (blue) also runs perpendicular through the device, 60 µm above the channels. (C) Photograph of a 3D printed device. (D-E) SEM images of an LMA monolith polymerized within a 70 x 50 μm^2 channel, demonstrating wall adhesion and porosity.

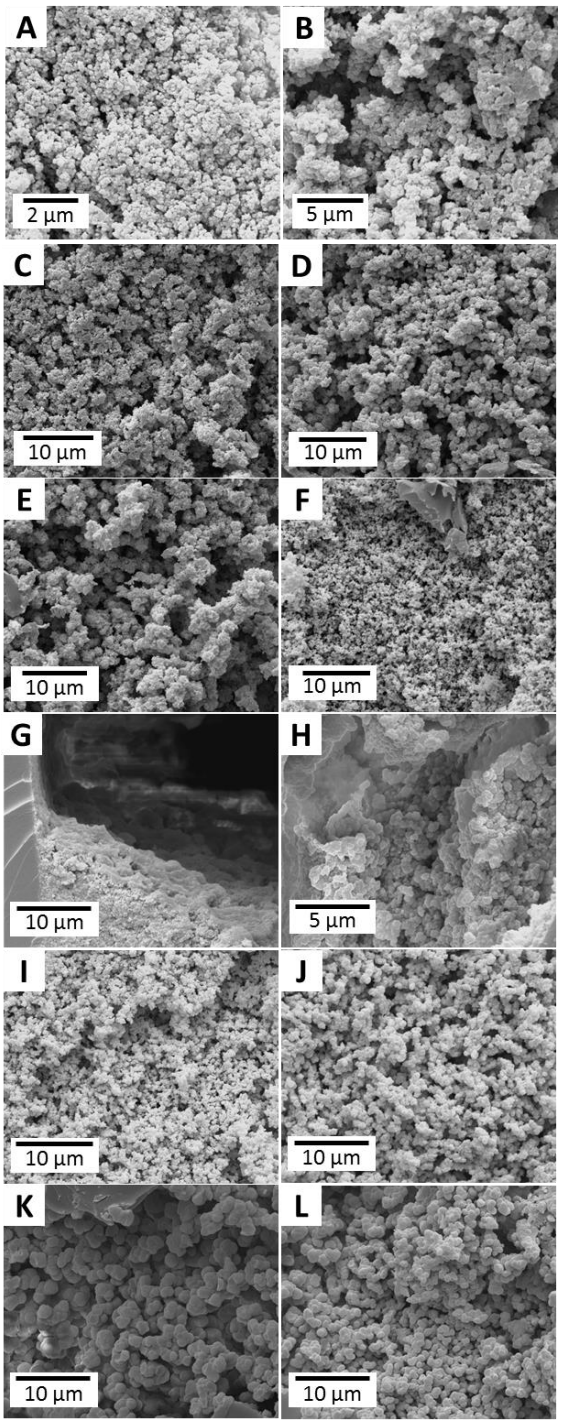

Figure 2. SEM images of monoliths in 3D printed microfluidic channels. Each image letter corresponds to the monolith formulation given in Table 2.

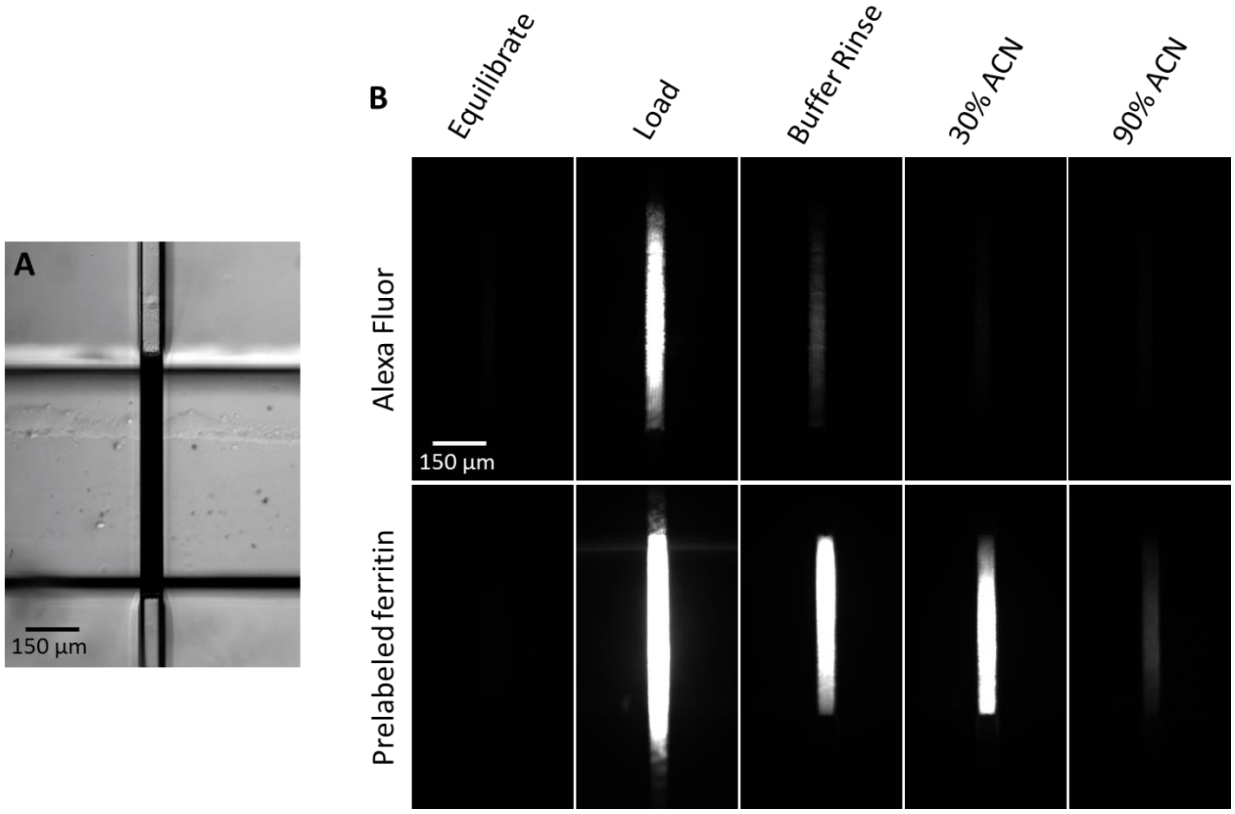

Figure 3. Images of reversed-phase LMA monoliths during SPE. (A) Photograph of a monolith showing formation and confinement within the polymerization window (visible as the two dark lines running horizontally through the image). (B) Fluorescence images of successive steps during SPE experiments including buffer equilibration, sample loading (Alexa Fluor or ferritin), buffer rinse, 30% ACN elution, and 90% ACN elution. Scale is the same in all images.

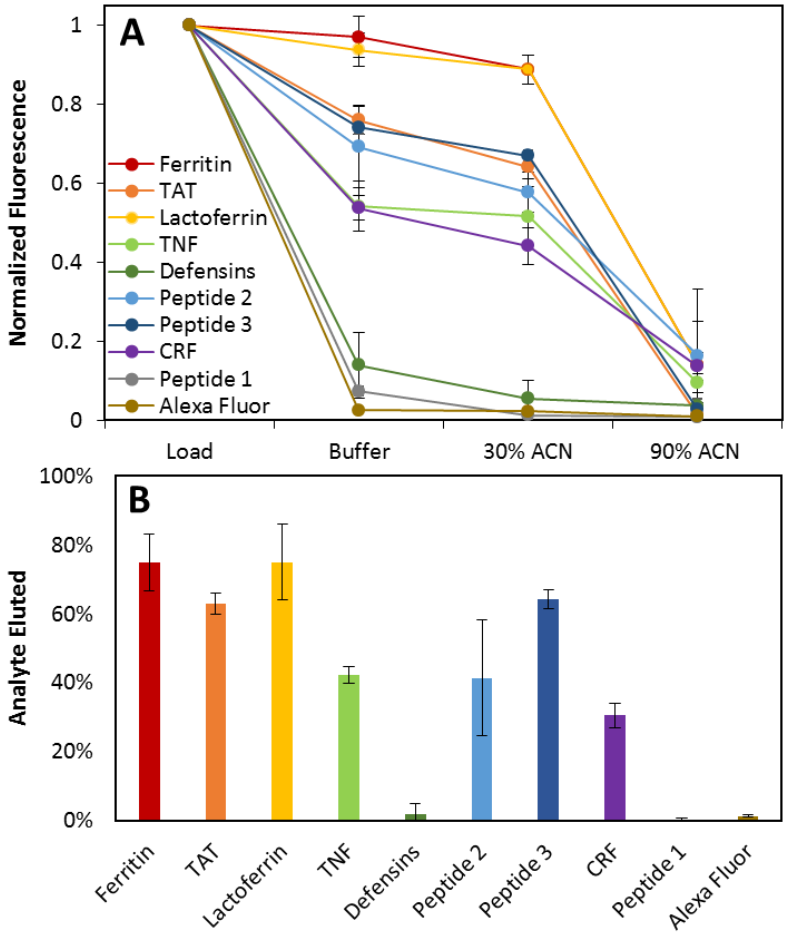

Figure 4. SPE of Alexa Fluor and prelabeled PTB biomarkers on LMA reversed-phase monoliths in 3D printed microfluidic devices. (A) Normalized fluorescent signal on the monolith after the load, buffer rinse, 30% ACN, and 90% ACN elution steps. (B) Percent of the total retained analyte eluted with 90% ACN. Error bars represent the standard deviation of three replicates.

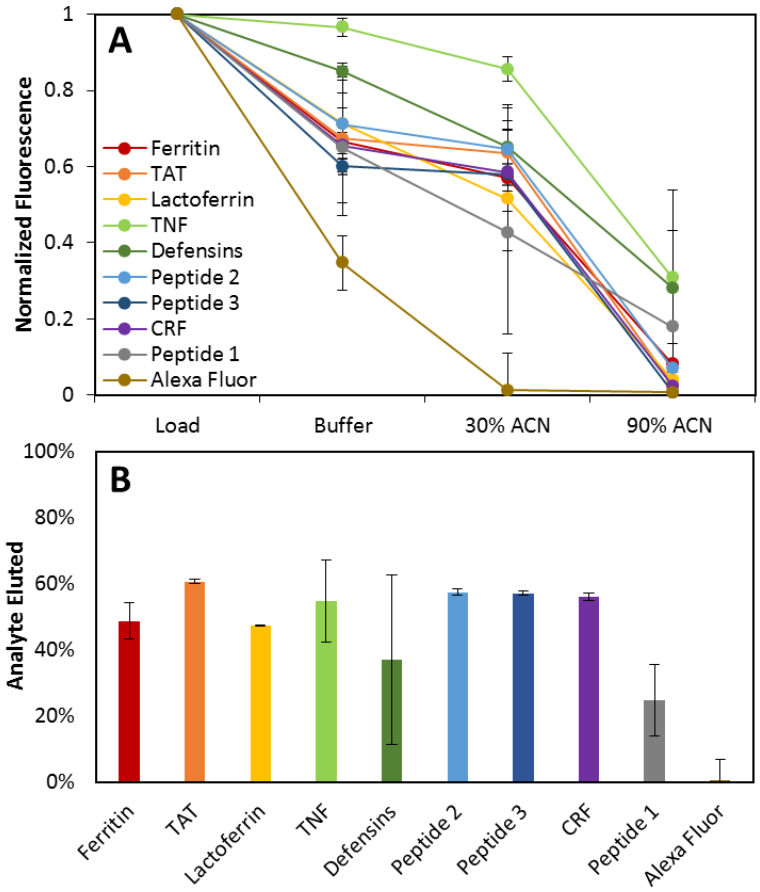

Figure 5. SPE and on-chip fluorescent labeling of PTB biomarkers on LMA reversed-phase monoliths. (A) Normalized fluorescent signal on the monolith after loading/labeling, buffer rinse, 30% ACN, and 90% ACN elution steps. (B) Percent of the total retained analyte eluted with 90% ACN.

Graphical Abstract Figure